# Monolithic crystalline silicon solar cells with SiN layers doped with Tb3+ and Yb3+ rare-earth ions

Ing-Song Yu, Shao-Chun Wu, Lucile Dumont, Julien Cardin, Christophe Labbé, Fabrice Gourbilleau

# Monolithic crystalline silicon solar cells with $SiN_x$ layers doped with $Tb^{3+}$ and $Yb^{3+}$ rare-earth ions☆

Ing-Song Yu [a, *], Shao-Chun Wu [a], Lucile Dumont [b], Julien Cardin [b], Christophe Labbé [b], Fabrice Gourbilleau [b]

[a] Department of Materials Science and Engineering, National Dong Hwa University, Hualien, 97401, Taiwan, China
[b] CIMAP CNRS/CEA/ENSICAEN/Université de Caen Normandie, 6 Boulevard Maréchal Juin, 14050 Caen, Cedex, 4, France

ARTICLE INFO

*Article history:*
Received 28 May 2018
Received in revised form
25 July 2018
Accepted 26 July 2018
Available online xxx

*Keywords:*
Crystalline silicon solar cell
Spectrum conversion
Silicon nitride
Down-shifting
Rare-earth ion
Anti-reflection coating

ABSTRACT

In this study, we propose the fabrication of monolithic crystalline silicon solar cells with $Tb^{3+}$ and $Yb^{3+}$-doped silicon nitride ($SiN_x$) layers by low-cost screen-printing methods. The performances of c-Si solar cells can be enhanced by rare-earth ions doped $SiN_x$ layers via the mechanism of spectrum conversion. These $SiN_x$ doped and codoped thin films were deposited by reactive magnetron co-sputtering and integrated as the antireflection coating layers in c-Si solar cells. The characterizations of $SiN_x$, $SiN_x$:$Tb^{3+}$ and $SiN_x$:$Tb^{3+}$-$Yb^{3+}$ thin films were conducted by means of photoluminescence, Rutherford backscattering spectroscopy, Ellipsometry spectroscopy and Fourier transform infrared measurements. Their composition and refractive index was optimized to obtain good anti-reflection coating layer for c-Si solar cells. Transmission electron microscopy performs the uniform coatings on the textured emitter of c-Si solar cells. After the metallization process, we demonstrate monolithic c-Si solar cells with spectrum conversion layers, which lead to a relative increase by 1.34% in the conversion efficiency.



## 1. Introduction

Energy crisis and global warming are two important issues in twenty-first century. Solar energy is one of the solutions to solve these problems. Now, many materials are proposed for photovoltaic technologies such as Si, GaAs, CdTe and CIGS.[1] In industry, crystalline silicon (c-Si) solar cell is still the mainstream among the various technologies of solar cells. The conversion efficiency of c-Si solar cells can be improved by reducing optical loss, carrier recombination loss and electrical loss. So far, the best experimental c-Si solar cells fabricated in the laboratories have achieved conversion efficiency of 25%.[2,3] Beside these above mentioned loss mechanisms, the main energy loss of c-Si for converting solar energy to electricity is the mismatch of the solar spectrum and the band gap energy of Si. The sub-bandgap photons ($E < 1.1$ eV) cannot be absorbed by Si solar cells. The excess energy of high energetic photons ($E > 1.1$ eV) is lost via non-radiative relaxation in the form of heat. The fundamental spectral loss that limits the theoretical maximum efficiency of single junction Si device is around 31%, which is known as the Shockley-Queisser efficiency limit.[4] To break this limitation, several methods were proposed, such as tandem solar cells, intermediate-band cells, hot carrier cells and spectrum conversion. All those methods are clustered in the third generation photovoltaic cells.[5]

To increase conversion efficiency of a single junction solar cell, such as c-Si solar cells, spectrum conversion is a good method to modify solar spectrum by means of down-conversion (i.e. quantum cutting), down-shifting or up-conversion. Down-conversion is the process of splitting one high energy photon into more than one lower energy photons which can be absorbed by the cell. Down-shifting is the process of absorbing one high energy photon and releasing one lower energy photons for better absorption. Up-conversion is the process to combine two low energy photons into one absorbable photon by the Si solar cell. Traditional single junction c-Si solar cells are fabricated by thermal diffusion and screen printing processes for a low-cost approach. External quantum efficiency (EQE) of c-Si solar cells is still poor at short-wavelength range (from 300 to 500 nm) because of the recombination at the surface layer with heavily phosphorus-doped emitter

* Foundation item: Project supported by Ministry of Science and Technology, Taiwan (MOST 105-2911-I-259-501), the French Agence Nationale de Recherche through the GENESE Project (ANR-13-BSS09-0020-01), and the French Ministry of Research through the ORCHID Project (33572XF).

* Corresponding author.
E-mail address: isyu@gms.ndhu.edu.tw (I.-S. Yu).

and increased reflectance and absorption from antireflection coating (ARC). However, luminescent down-conversion and down-shifting materials have been proposed for improving the poor spectral response of c-Si solar cells to short wavelength light. These materials can also decrease slightly the operational temperature due to electron-hole pair thermalization losses in the cells.[6–9]

Rare-earth ions (lanthanide ions) doped materials can absorb and emit light via the energy levels of the active ions. Those rare-earth ions may be praseodymium ($Pr^{3+}$), erbium ($Er^{3+}$), europium ($Eu^{3+}$), samarium ($Sm^{3+}$), cerium ($Ce^{3+}$) and terbium ($Tb^{3+}$) in different host materials. These luminescent materials have been used in the lighting, display panel, photocatalytic and photovoltaic technologies.[10–17] For a better integration with c-Si solar cell process, rare-earth ions were inserted in a specific oxide or nitride environment. In the material, those rare-earth ions are mostly stable as divalent or trivalent cations and can efficiently convert UV radiation into visible light as down-shifting layers.[18] Besides, down-conversion layers using rare earth ion pairs can provide the energy transfer from one rare-earth ion to another one such as in the $Tb^{3+}$—$Yb^{3+}$, $Pr^{3+}$—$Yb^{3+}$ or $Nd^{3+}$—$Yb^{3+}$ codoped systems.[19–23] Thus the down-shifting and down-conversion layers can theoretically be used to improve the performance of c-Si solar cell by reducing the thermalization process.

As we know, silicon nitride ($SiN_x$) thin film has been used as ARC layer at the front side of p-type c-Si solar cells in industry.[24] In this report, $Tb^{3+}$-doped and $Tb^{3+}$-$Yb^{3+}$-codoped $SiN_x$ thin films were deposited by reactive radio frequency magnetron co-sputtering using three different metallic targets: silicon, terbium, and ytterbium, under a mixture of argon and nitrogen plasma. In addition, $SiN_x$:$Tb^{3+}$ thin film was integrated into c-Si solar cell as the down-shifting layer. $SiN_x$:$Tb^{3+}$-$Yb^{3+}$ thin film was integrated into c-Si solar cell as the down-conversion layer. Finally, a monolithic c-Si solar cell with spectrum conversion layers was demonstrated, and the enhanced performance of c-Si solar cells with these layers was investigated.

## 2. Experimental

In this work, $SiN_x$, $SiN_x$:$Tb^{3+}$ and $SiN_x$:$Tb^{3+}$-$Yb^{3+}$ layers were deposited by reactive magnetron co-sputtering in nitrogen-rich plasma. For the deposition parameters, the power density applied on the Si target was fixed at 4.5 W/cm$^2$, and the gas fluxes were $1.35 \times 10^{-2}$ Pa·m$^3$/s for argon and $3.38 \times 10^{-3}$ Pa·m$^3$/s for nitrogen. The deposition operated at plasma pressure 0.40 Pa, and the substrate temperature was fixed at 200 °C. The doping of rare-earth ions was controlled by the power densities separately applied on the terbium and ytterbium metal targets. The deposition time was adjusted to obtain 80 nm-thick films which requires an ARC layer with a refractive index around 2.2 (at 1.95 eV). The optimized photoluminescence emission in the visible range for the $Tb^{3+}$ ions or in the infrared one for the $Yb^{3+}$ ions has been achieved after an annealing process at 850 °C. The composition of the produced layers was determined by Rutherford backscattering spectroscopy (RBS) while refractive index and thickness were deduced from ellipsometry spectroscopy experiments. Fourier transform infrared measurement (FTIR) was employed to investigate the Si—N bond in the layers.

Fig. 1 shows the process flow of monolithic c-Si solar cells with two different spectrum conversion layers. First, 200-μm p-type Si wafer was cleaned by KOH solution to remove the saw damage as well as for surface texturing. Second, Si doped phosphorus was conducted by thermal diffusion at 850 °C for 30 min. Then, isolation etching process was provided to remove the edge and backside n-type Si. Then, samples were cut into the size of 3.5 cm × 3.5 cm. Prior to spectrum conversion layers deposition, the samples were cleaned by HF solution to remove native oxide layer on the surface. Three different thin films were then deposited by sputtering[16] and followed by a thermal annealing process to recover the non-radiative paths in these layers. Finally, the metallization of c-Si solar cells, consisting in a screen-printing of metals and a co-firing process, was conducted. After these processes, a monolithic c-Si solar cell with spectrum conversion layers was obtained as is shown by the schematic diagram in Fig. 2. This report consists of three parts: the characterization of spectrum conversion layers, optical properties of spectrum conversion layers on c-Si solar cells, and the performances of solar cells with these layers.

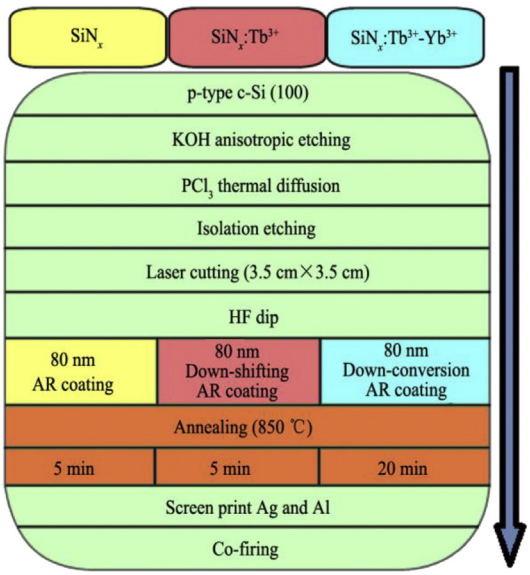


**Fig. 1.** Process flow of c-Si solar cells with spectrum conversion layers.

## 3. Results and discussion

### 3.1. Characterizations of $SiN_x$, $SiN_x$:$Tb^{3+}$ and $SiN_x$:$Tb^{3+}$-$Yb^{3+}$ layers

The results of the RBS measurements for those three samples are shown in Table 1. The composition of $SiN_x$ in the three layers is close to the stoichiometric composition ($Si_3N_4$) even when rare-earth ions are added. The doping concentrations of $Tb^{3+}$ and $Yb^{3+}$ ions in the matrix achieved by RBS analysis are also exhibited in Table 1.

Fig. 3 shows the refractive index at 1.95 eV for the three layers. The blue line represents the refractive index of the stoichiometric silicon nitride, $Si_3N_4$. We can find that the refractive index increases

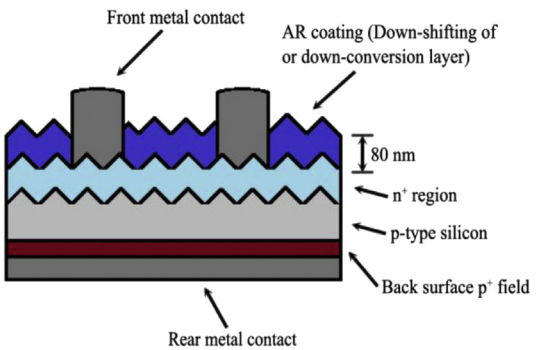


**Fig. 2.** Schematic diagram of c-Si solar cells with spectrum conversion layers.

**Table 1**
The composition analysis of $SiN_x$ and doped $SiN_x$ layers by RBS (at%).

| Samples | Si | N | Tb | Yb |
|---|---|---|---|---|
| $SiN_x$ | 43 | 57 | – | – |
| $SiN_x$:$Tb^{3+}$ | 42 | 56 | 1.5 | – |
| $SiN_x$:$Tb^{3+}$-$Yb^{3+}$ | 39.5 | 52.7 | 5.8 | 2 |

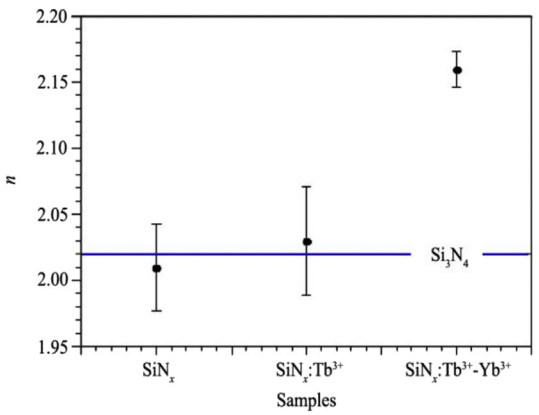


**Fig. 3.** Refractive index of three layers at 1.95 eV deduced from Ellipsometry analysis.

when the matrix is doped with one or two types of rare-earth ions. The doping of 1.5 at% terbium in the $SiN_x$ matrix raises refractive index 0.02. The doping of 7.8 at% rare-earth ions leads to an increase of the refractive index 0.14. These are still in the acceptable range (from 2.0 to 2.2) for the application in c-Si solar cells.

The FTIR analysis was conducted on the three samples and the results are shown in Fig. 4. The two peaks present the longitudinal optical (LO) and the transversal optical (TO) modes of the asymmetric Si–N bond. The position of the TO peak does not vary between the samples. The LO peak's position shifts to the low wavenumbers when rare-earth ions are inserted in the $SiN_x$ matrix. This shift may be attributed to a decrease in the silicon content compared with the nitrogen one, or to an increasing stress in the matrix due to the increasing insertion of rare-earth ions in the matrix.[25] In addition, the range of wavenumber between those two peaks (1100–900 $cm^{-1}$) may be related to the lattice vibration that is a signature of the matrix disorder. Fig. 4 shows that the intensity difference between this part of the spectrum and the two peaks became smaller when one then two types of rare-earth ions are

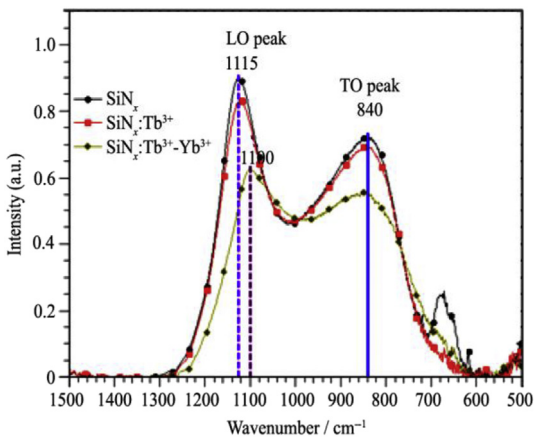


**Fig. 4.** FTIR spectra for the three different layers: the two peaks present LO and TO modes of the asymmetric Si–N bond.

incorporated in the matrix. Thus, the shift of the LO peak towards the low wavenumbers should be attributed to the increase of disorder due to the insertion of rare-earth ions.

### *3.2. Microstructures and optical properties of these layers on textured emitter*

After the fabrication of c-Si solar cells, these layers were integrated in monolithic c-Si solar cells. Fig. 5 shows the images of cross-section transmission electron microscopy. The microstructure of $SiN_x$ doped with $Tb^{3+}$-$Yb^{3+}$ thin films can be observed on the textured Si surface by TEM observations. The layers were uniformly coated on the textured emitter of c-Si solar cells with the thickness around 70 nm.

The optical properties of these layers can be characterized by photoluminescence, and reflectance measurements. In Fig. 6, the emission of $SiN_x$ layer is very weak compared with the doped layers. However, it emits from and below 488 nm allowing the energy transfer from the matrix to the terbium ions. Such sensitization effect of rare-earth ions allow to overcome their low absorption cross section as already demonstrated in such a nitride based matrix. In addition, it has been determined that this transfer most likely occurs toward the high energy levels of the terbium ions before undertaking relaxation to the $^5D_4$ energy level as shown by An et al.[16,18] $Tb^{3+}$ ions in the $SiN_x$ matrix emit from 500 to 630 nm as displayed in Fig. 6 which exhibits the four characteristic peaks of the terbium at 629, 594, 550 and 493 nm that correspond to the $^5D_4$ to $^7F_3$, $^7F_4$, $^7F_5$, and $^7F_6$ energy transfers. The UV light can thus be absorbed by matrix and then transferred to the $Tb^{3+}$ ions that will then transfer the converted light to the Si. Therefore, $SiN_x$:$Tb^{3+}$ can be a down-shifting layer for c-Si solar cell. For the $SiN_x$:$Tb^{3+}$-$Yb^{3+}$ thin film, this layer only presents the characteristic peak of the $Yb^{3+}$ at 990 nm which originates from the $^2F_{5/2}$ to $^2F_{7/2}$ energy transfer. The spectra show a mechanism of spectral down-conversion, energy transfer from one rare-earth ion to two other rare-earth ions. Thus, $SiN_x$ codoped with $Tb^{3+}$-$Yb^{3+}$ ions can be a down-conversion layer for c-Si solar cell.

The reflectivity of these layers on textured emitter is important for c-Si solar cells because these layers also play the role of an ARC layer. Fig. 7 shows the reflectance as a function of the wavelength. The minimum of reflectance is between 400 and 500 nm. The reflectance increases at shorter wavelength, and a bump rising of reflectance at around 1050 nm is observed. To overall justify the ARC performance of our layers for solar cells, we can calculate the weighed average reflectance (WAR) at AM1.5G in the range of 300 and 1200 nm. The WAR value of these layers on the textured Si is around 6%, which shows the good light harvesting as ARC layers for c-Si solar cells.[26,27]

### *3.3. Performances of c-Si solar cells with these three layers*

In previous section, the optical properties of rare-earth ion doped $SiN_x$ layers on textured emitters can be spectrum conversion and ARC layers for c-Si solar cells. We move forward to realize the performance of monolithic c-Si solar cells with these layers. After the process of metallization, external quantum efficiency (EQE) measurement was employed to get the short-circuit current density ($J_{sc}$), and pseudo $I$–$V$ curve without the effect of series resistance could be obtained by Sinton's Suns $V_{oc}$ measurement.[28,29] Fig. 8 shows the $I$–$V$ curves of three cells, and inset is the zoom of curves. The photovoltaic performances of these cells are summarized in Table 2. To compare with the c-Si solar cell without rare-earth ion doping, the performances of c-Si solar cell with $SiN_x$ doped with $Tb^{3+}$ or codoped with $Tb^{3+}$–$Yb^{3+}$ have enhancement in short-circuit current density and open-circuit voltage ($V_{oc}$). The conversion efficiency is from 17.13% to 17.31% for the down-shifting

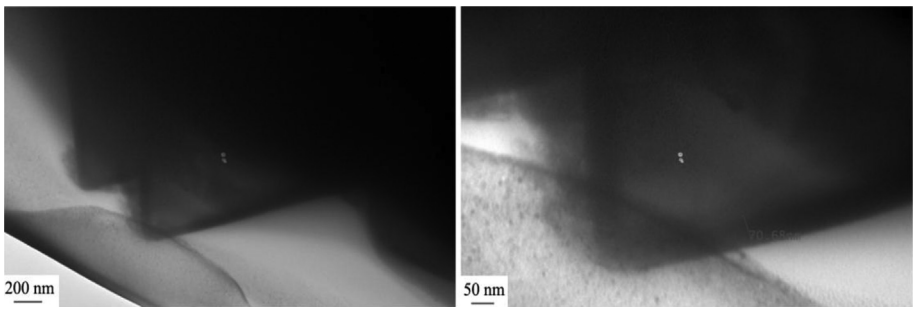


**Fig. 5.** TEM images of $SiN_x$ doped with $Tb^{3+}$- $Yb^{3+}$ on textured emitters.

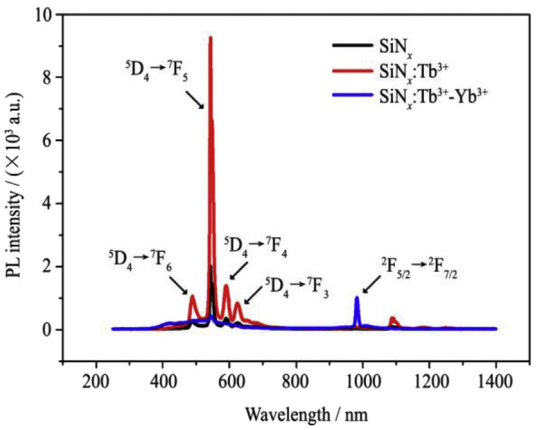


**Fig. 6.** PL measurements equipped with a 325 nm laser for the three layers on textured emitters of solar cells.

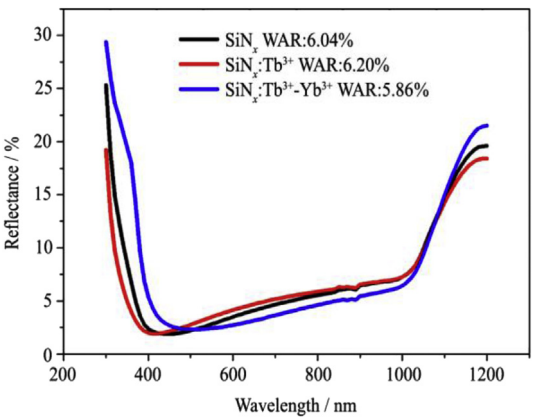


**Fig. 7.** Reflectance of three layers deposited on textured emitters.

layer ($SiN_x$ doped with $Tb^{3+}$). The conversion efficiency is from 17.13% to 17.36% for the down-conversion layer ($SiN_x$ codoped with $Tb^{3+}$—$Yb^{3+}$).

The performance enhancement of Si solar cells both comes from the anti-reflection and spectrum conversion effects of these films. From the WAR values of three different layers as 6.04%, 6.20% and 5.86%, the corresponding weighed average transmission of 93.96%, 93.80% and 94.14% can be obtained. To normalize the effect of anti-reflection coating, the ratios of conversion efficiency to transmission can be calculated as 18.23%, 18.45% and 18.44%, respectively. The $SiN_x$ films doped with $Tb^{3+}$ or codoped with $Tb^{3+}$—$Yb^{3+}$ can enhance the performance of c-Si solar cells due to the effect of spectrum conversion.

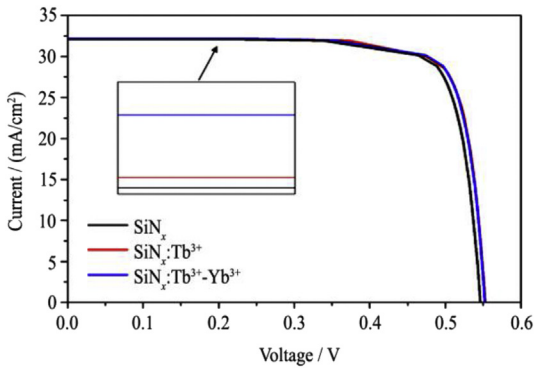


**Fig. 8.** Pseudo *I-V* curves for three c-Si solar cells with $SiN_x$, $SiN_x$:$Tb^{3+}$ and $SiN_x$:$Tb^{3+}$-$Yb^{3+}$ layers, respectively.

**Table 2**
Photovoltaic performances of c-Si solar cells with $SiN_x$, $SiN_x$:$Tb^{3+}$ and $SiN_x$:$Tb^{3+}$-$Yb^{3+}$ layers.

| Samples | $J_{sc}$ (mA/cm$^2$) | $V_{oc}$ (V) | Pseudo FF (%) | Pseudo Efficiency (%) | Efficiency to normalized transmission (%) |
|---|---|---|---|---|---|
| $SiN_x$ | 32.091 | 0.546 | 0.804 | 17.13 | 18.23 |
| $SiN_x$:$Tb^{3+}$ | 32.098 | 0.552 | 0.803 | 17.31 | 18.45 |
| $SiN_x$:$Tb^{3+}$-$Yb^{3+}$ | 32.165 | 0.552 | 0.806 | 17.36 | 18.44 |

## 4. Conclusions

A monolithic c-Si solar cell with spectrum conversion layers was demonstrated with $Tb^{3+}$ doped $SiN_x$ and $Tb^{3+}$-$Yb^{3+}$ codoped $SiN_x$ thin films. These thin films can not only play the role as anti-reflection coating, but also improve the performances of c-Si solar cells due to the spectrum conversion effects (down-shifting and down-conversion). From the characterizations of these films, their composition and refractive index are close to stoichiometric $Si_3N_4$. The layers with the thickness of 70 nm are uniformly coated on the textured emitter of c-Si solar cells. For the down-shifting layer, the UV light can be absorbed by matrix and then transfer to the $Tb^{3+}$ ions. For down-conversion effect layer, energy transfers from one rare-earth ion to two other rare-earth ions from the PL measurements.

## References

1. Green MA, Emery K, Hishikawa Y, Wartra W, Dunlup ED. Solar cell efficiency tables (Version 45). *Prog Photovolt Res Appl*. 2015;23:1.
2. Green MA. The path to 25% silicon solar cell efficiency: history of silicon cell evaluation. *Prog Photovolt Res Appl*. 2009;17:183.
3. Saga T. Advances in crystalline silicon solar cell technology for industrial mass production. *NPG Asia Mater*. 2010;2(3):96.

4. Shockley W, Queisser HJ. Detailed balance limit of efficiency of p-n junction solar cells. *J Appl Phys*. 1961;32:510.
5. Brown GF, Wu J. Third generation photovoltaics. *Laser Photon Rev*. 2009;3(4): 394.
6. Richards BS. Luminescent layers for enhanced silicon solar cell performance: down-conversion. *Sol Energy Mater Sol Cells*. 2006;90:1189.
7. Sewell RH, Clark A, Arkum E, Smith RS, Semans S, Jamora A, et al. Epitaxial rare-earth oxide layers for enhancement of silicon based solar cells. In: *Proc. 24th EUPVSEC*. 2009:326.
8. Klampaftis E, Ross D, McIntosh KR, Richards BS. Enhancing the performance of solar cells via luminescent down-shifting of the incident spectrum: a review. *Sol Energy Mater Sol Cells*. 2009;93:1182.
9. Chen YC, Huang WY, Chen TM. Enhancing the performance of photovoltaic cells by using down-converting $KCaGd(PO_4)_2:Eu^{3+}$ phosphors. *J Rare Earths*. 2011;29:907.
10. Strumpel C, McCann M, Beaucarne G, Arkhipov V, Svrcek V, del Canizo C, et al. Modifying the solar spectrum to enhance silicon solar cell efficiency — an overview of available materials. *Sol Energy Mater Sol Cells*. 2007;91:238.
11. Kenyon AJ. Recent developments in rare-earth doped materials for optoelectronics. *Prog Quantum Electron*. 2002;26:225.
12. Shao GJ, Luo CG, Kang J, Zhang H. Luminescent down shifting effect of Ce-doped yttrium aluminum garnet thin films on solar cells. *Appl Phys Lett*. 2015;107:253904.
13. Ho WJ, Yang GC, Shen YT, Deng YJ. Improving efficiency of silicon solar cells using europium-doped silicate-phosphor layer by spin-on film coating. *Appl Surf Sci*. 2016;265:120.
14. Xie RJ, Hirosaki N, Li Y, Takeda T. Rare-earth activated nitride phosphors: synthesis, luminescence and applications. *Materials*. 2010;3:3777.
15. Prezas PR, Graca MPF, Soares MJ, Kumar JS. Optical and structural properties of $(70\text{-}x\text{-}y)TeO_2\text{-}20WO_3\text{-}10Y_2O_3\text{-}xEr_2O_3\text{-}yYb_2O_3$ glasses. *Appl Surf Sci*. 2015;336:28.
16. An YT, Labbé C, Morales M, Gourbilleau F. Fabrication and photoluminescence properties of Tb-doped nitrogen-rich silicon nitride films. *Phys Status Solidi C*. 2012;9(10−11):2207.
17. Yu YG, Chen G, Zhou YS, Han ZH. Recent advances in rare-earth elements modification of inorganic semiconductor-based photocatalysts for efficient solar energy conversion: a review. *J Rare Earths*. 2015;33:453.
18. An YT, Labbé C, Cardin J, Morales M, Gourbilleau F. Highly efficient infrared quantum cutting in $Tb^{3+}$-$Yb^{3+}$ codoped silicon oxynitride for solar cell applications. *Adv Opt Mater*. 2013;1:855.
19. Dumont L, Benzo P, Cardin J, Yu IS, Labbé C, Marie P, et al. Down-shifting Si-based layer for Si solar applications. *Sol Energy Mater Sol Cells*. 2017;169:132.
20. Huang XY, Zhang QY. Efficient near-infrared down conversion in $Zn_2SiO_4$: $Tb^{3+}$,$Yb^{3+}$ thin films. *J Appl Phys*. 2009;105, 053521.
21. Song P, Jiang C. Modeling of wavelength down conversion based on $Nd^{3+}$-$Yb^{3+}$ system for improving c-Si solar cell performance. *J Opt*. 2013;15:025002.
22. Van Sark WGJHM. Simulating performance of solar cells with spectral down-shifting layers. *Thin Solid Films*. 2008;516:6808.
23. Dumont L, Cardin J, Benzo P, Carrada M, Labbé C, Richard AL, et al. $SiN_x$:$Tb^{3+}$-$Yb^{3+}$, an efficient down-conversion layer compatible with a silicon solar cell process. *Sol Energy Mater Sol Cells*. 2016;145:84.
24. Zhou HP, Wei DY, Xu LX, Guo YN, Xiao SQ, Huang YS, et al. Low temperature $SiN_x$:H films deposited by inductively coupled plasma for solar cell applications. *Appl Surf Sci*. 2013;264:21.
25. Huang L, Hipps KW, Dickinson JT, Mazur U, Wang XD. Structure and composition studies for silicon nitride thin films deposited by single ion beam sputter deposition. *Thin Solid Films*. 1997;299:104.
26. Park H, Kwon S, Lee JS, Lim HJ, Yoon S, Kim D. Improvement on surface texturing of single crystalline silicon for solar cells by saw-damage etching using an acidic solution. *Sol Energy Mater Sol Cells*. 2009;93:1773.
27. Yu IS, Wang YW, Cheng HE, Yang ZP, Lin CT. Surface passivation and antireflection behavior of ALD $TiO_2$ on n-type silicon for solar cells. *Int J Photoenergy*. 2013;V2013:431614.
28. Open photovoltaics analysis platform. Available online: http://opvap.com/eqe.php. Accessed 14 May 2018.
29. Kerr MJ, Cuevas A, Sinton RA. Generalized analysis of quasi-steady-state and transient decay open circuit voltage measurements. *J Appl Phys*. 2002;91:399.